

SiliconPV: 17-20 April 2011, Freiburg, Germany

High-rate atomic layer deposition of Al_2O_3 for the surface passivation of Si solar cells

Florian Werner^{a*}, Walter Stals^b, Roger Görtzen^b, Boris Veith^a, Rolf Brendel^{a,c},
Jan Schmidt^{a,c}

^a*Institute for Solar Energy Research Hamelin (ISFH), Am Ohrberg 1, 31860 Emmerthal, Germany*

^b*SoLayTec, Dillenburgerstraat 9G, 5652 AM Eindhoven, The Netherlands*

^c*Institute of Solid-State Physics, University of Hanover, Appelstrasse 2, 30167 Hannover, Germany*

Abstract

High-rate spatial atomic layer deposition (ALD) enables an industrially relevant deposition of high-quality aluminum oxide (Al_2O_3) films for the surface passivation of silicon solar cells. We demonstrate a homogeneous surface passivation at a deposition rate of ~ 30 nm/min on 15.6×15.6 cm² silicon wafers of 10 nm thick Al_2O_3 layers deposited in a novel inline spatial ALD system. The effective surface recombination velocity on *n*-type Czochralski-grown (Cz) silicon wafers is shown to be virtually independent of injection level. Surface recombination velocities below 2.9 cm/s and an extremely low interface state density below 8×10^{10} eV⁻¹cm⁻² are achieved. We demonstrate that the novel inline spatial ALD system provides the means to integrate Al_2O_3 passivation layers into industrial solar cells.

© 2011 Published by Elsevier Ltd. Selection and/or peer-review under responsibility of SiliconPV 2011.

Keywords: Silicon; Surface passivation; Aluminum oxide; Spatial ALD;

1. Introduction

Aluminum oxide (Al_2O_3) deposited by atomic layer deposition (ALD) provides an outstanding level of surface passivation on both *n*- and *p*-type crystalline silicon [1-3]. Although Al_2O_3 is an ideal choice for the rear surface passivation of silicon solar cells [4], its integration into industrial solar cells is hampered by a low throughput. Conventional ALD reactors limit the deposition rate to < 2 nm/min and require extensive handling times. Recently, a spatial ALD concept was proposed [5], which enables deposition at

* Corresponding author. Tel.: +49-5151-999-314; fax: +49-5151-999-400.

E-mail address: werner@isfh.de.

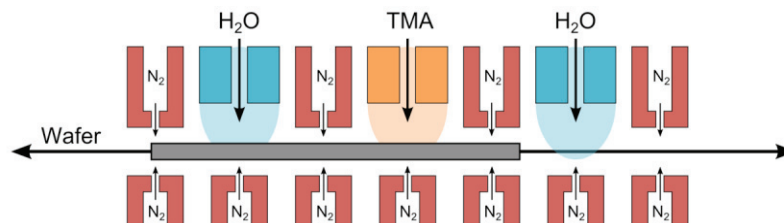


Fig. 1. Sketch of the spatial ALD concept [5]. The TMA and water half-reaction zones are separated by nitrogen curtains. Contactless transport of the wafer is facilitated by nitrogen gas bearings below the wafer.

atmospheric pressure with deposition rates of up to 70 nm/min. The potential of the spatial ALD concept was demonstrated on a proof-of-principle tool on small areas [6]. In this work we investigate the surface passivation with Al₂O₃ deposited by a novel inline spatial ALD system on large area (15.6×15.6 cm²) silicon wafers at a deposition rate of ~30 nm/min. We demonstrate that spatial ALD provides the means to integrate Al₂O₃ passivation layers into industrial solar cells.

2. High-rate spatial atomic layer deposition

In an ALD process a highly conformal, pin-hole free monolayer-by-monolayer coating is achieved by two alternating self-limiting half-reactions of the precursor molecules. In the first half-reaction trimethyl-aluminum (TMA, [Al(CH₃)₃]₂) molecules react with hydroxyl (–OH) groups attached to the surface, until a saturation of available reaction sites is reached. In the second half-reaction the surface is oxidized by water vapor (*thermal ALD*) or in an oxygen plasma (*plasma-assisted ALD*) to form aluminum oxide. A separation of the half-reactions is conventionally implemented by alternate dosing of the process gases combined with an intermediate purging and pumping of the deposition chamber, which limits the growth rate to < 2 nm/min. In a *spatial ALD* [5] process both half-reactions are *spatially* separated, as shown by the sketch in Fig. 1. The wafers move contactlessly on nitrogen gas bearings and pass TMA and water vapor inlets sealed off by a flow of pressurized nitrogen, forming isolated reaction zones. The wafers move back and forth underneath the reactor head, each passage depositing one monolayer of Al₂O₃. In this concept no intermediate pumping steps are required, which significantly reduces the duration of each ALD cycle. The deposition rate is determined by the cycle rate of the wafer in the reactor, enabling deposition rates of up to 70 nm/min. In a conventional ALD reactor operating under vacuum conditions, pump and vent times can severely limit the wafer throughput. As the spatial ALD concept works under atmospheric pressure, any pump or vent times are avoided.

A process development tool (PDT) manufactured by SoLayTec was employed to assess the passivation quality of Al₂O₃ films deposited by spatial ALD. In the PDT the wafer is heated to 200 °C in 6 seconds, and is then cycled through the core reactor sketched in Fig. 1 at a rate of 2 Hz, resulting in a deposition rate of 4 monolayers per second, or ~30 nm/min. If the desired number of ALD cycles – and correspondingly the desired layer thickness – is reached, the wafer is ejected from the core reactor and is cooled down for 30 seconds on a cooling track. During this time the next wafer can already be processed in the core reactor. We use 4 Ωcm *n*-type Czochralski-grown (Cz) silicon wafers with a size of 15.6 × 15.6 cm² (full-square), which were etched to a thickness of 180±15 μm in an aqueous KOH solution and received a standard RCA clean. Al₂O₃ films with a thickness of 10, 30 and 200 nm, respectively, were deposited on both wafer surfaces by spatial ALD, and were subsequently annealed at 350 °C for 30 min in a nitrogen ambient to activate the passivation. In addition, four wafers were passivated with 10 nm of Al₂O₃ deposited by plasma-assisted ALD in an Oxford FlexAL™ reactor and annealed at 425 °C for 15 min. These wafers serve as a reference, as Al₂O₃ deposited by plasma-assisted ALD is known to yield extremely low surface recombination velocities on lowly doped *n*-type silicon [2,3].

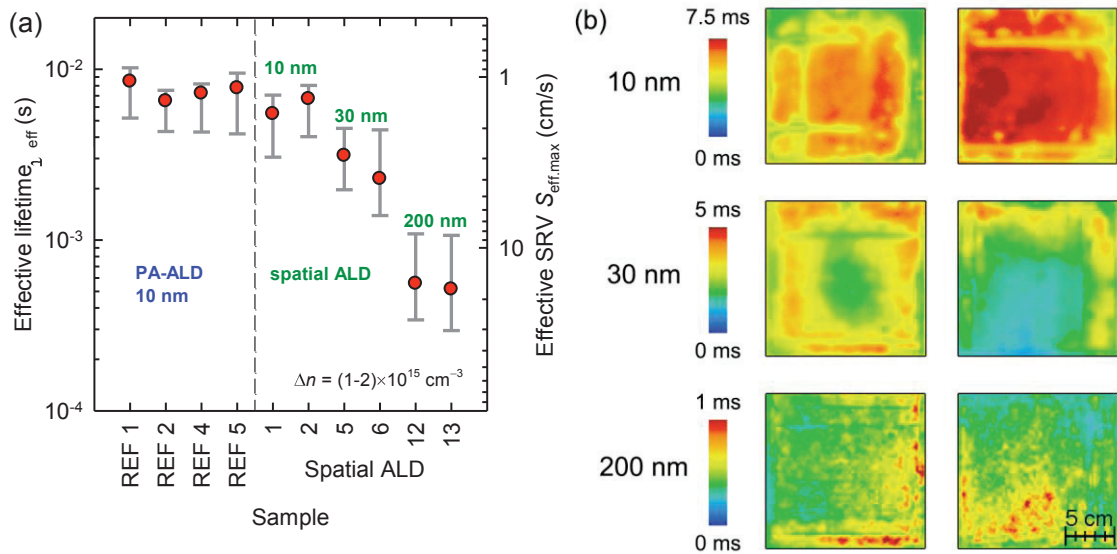


Fig. 2. (a) Effective lifetime τ_{eff} and maximum effective SRV $S_{\text{eff,max}}$ for Al₂O₃ thicknesses of 10, 30, and 200 nm deposited by spatial ALD, and 10 nm deposited by plasma-assisted ALD, respectively. The lifetime is calculated from the lifetime mappings shown in (b) by averaging over the wafer area, error bars denote the minimum and maximum values; (b) Spatially resolved lifetime mappings measured by dynamic ILM for 15.6×15.6 cm² *n*-type Cz-Si wafers passivated by spatial ALD.

3. Effective surface recombination velocity

A camera-based dynamic infrared lifetime mapping (ILM) technique [7] provides a fast analysis of the lateral uniformity of the surface passivation achieved by spatial ALD of Al₂O₃. In the dynamic ILM analysis, wafers are exposed to a constant illumination intensity, which has to be carefully set to compare lifetime mappings of different wafers at a similar injection density Δn . In addition it should be kept in mind that the local injection density Δn might vary over the wafer area. The injection-density-dependent effective lifetime $\tau_{\text{eff}}(\Delta n)$ is measured by transient photoconductance decay (PCD) using a Sinton Instruments WCT-120 lifetime tester in the transient mode, with the wafers centered over the sensor area. The corresponding maximum effective surface recombination velocity (SRV) $S_{\text{eff,max}}$ is calculated from the measured τ_{eff} using the equation $S_{\text{eff,max}} = W/(2 \tau_{\text{eff}})$ [8], where $W = 180 \mu\text{m}$ is the mean wafer thickness. The bulk lifetime was assumed to be infinite. We combine both measurement techniques – dynamic ILM and transient PCD – in this study in order to gain information about both the spatial variations and the injection density dependence of the effective lifetime τ_{eff} .

Figure 2(a) shows the effective lifetime τ_{eff} measured by dynamic ILM and averaged over the wafer area, excluding ~ 0.5 cm around the wafer edges. The error bars denote the minimum and maximum lifetime values recorded within this area. The spatially resolved lifetime mappings corresponding to the data points are shown in Fig. 2(b) for the samples passivated by spatial ALD. The reference wafers passivated by plasma-assisted ALD yield effective lifetimes at a mean injection density of $\Delta n = (1-2) \times 10^{15} \text{ cm}^{-3}$ between 4.2 and 10.2 ms, corresponding to a maximum effective SRV of $S_{\text{eff,max}} = 0.9 - 2.2$ cm/s. A comparable level of surface passivation is achieved with 10 nm of Al₂O₃ deposited by high-rate spatial ALD, yielding effective lifetimes between 3.1 and 8.1 ms ($S_{\text{eff,max}} = 1.1 - 2.9$ cm/s). A slight degradation of the effective lifetime along two parallel stripes might be attributed to the wafer handling prior to or during deposition. Adjustments to the wafer handling hence promise to further improve the already excellent surface passivation quality.

We observe a reduced effective lifetime for an Al₂O₃ thickness exceeding 10 nm. For a film thickness of 30 nm this effect is marginal, yielding effective lifetimes between 1.4 and 4.5 ms ($S_{\text{eff,max}} = 2.0 - 6.5 \text{ cm/s}$). For a film thickness of 200 nm, however, we measure significantly reduced effective lifetimes between 300 μs and 1.1 ms, corresponding to $S_{\text{eff,max}} = 8.2 - 30.5 \text{ cm/s}$. The reasons for the degradation of surface passivation quality with increasing film thickness are not yet fully understood and are currently under investigation. As this effect is absent prior to annealing of the lifetime samples, the degradation might be related to thermal stress and the accompanying damage to the Si/Al₂O₃ interface induced during thermal treatment. The reduced lifetime for thick Al₂O₃ layers, however, is of no concern for the industrial fabrication of solar cells, as such thick layers of Al₂O₃ are usually not desired. Superior optical properties and firing stability are obtained with a stack system comprising a thin (~10 nm) Al₂O₃ passivation layer deposited by ALD and a thicker capping layer, commonly of hydrogenated amorphous SiN_x deposited by plasma-enhanced chemical vapor deposition (PECVD) [9,10].

The dependence of the surface passivation quality on injection density Δn is addressed in Fig. 3. Figure 3(a) shows the effective lifetime τ_{eff} and maximum effective SRV $S_{\text{eff,max}}$ as a function of injection density Δn measured by transient PCD. In agreement with Fig. 2 the reference samples passivated by plasma-assisted ALD and the samples passivated with 10 nm Al₂O₃ deposited by spatial ALD show an excellent level of surface passivation. For thicker Al₂O₃ layers the effective lifetime is reduced. Independent of the

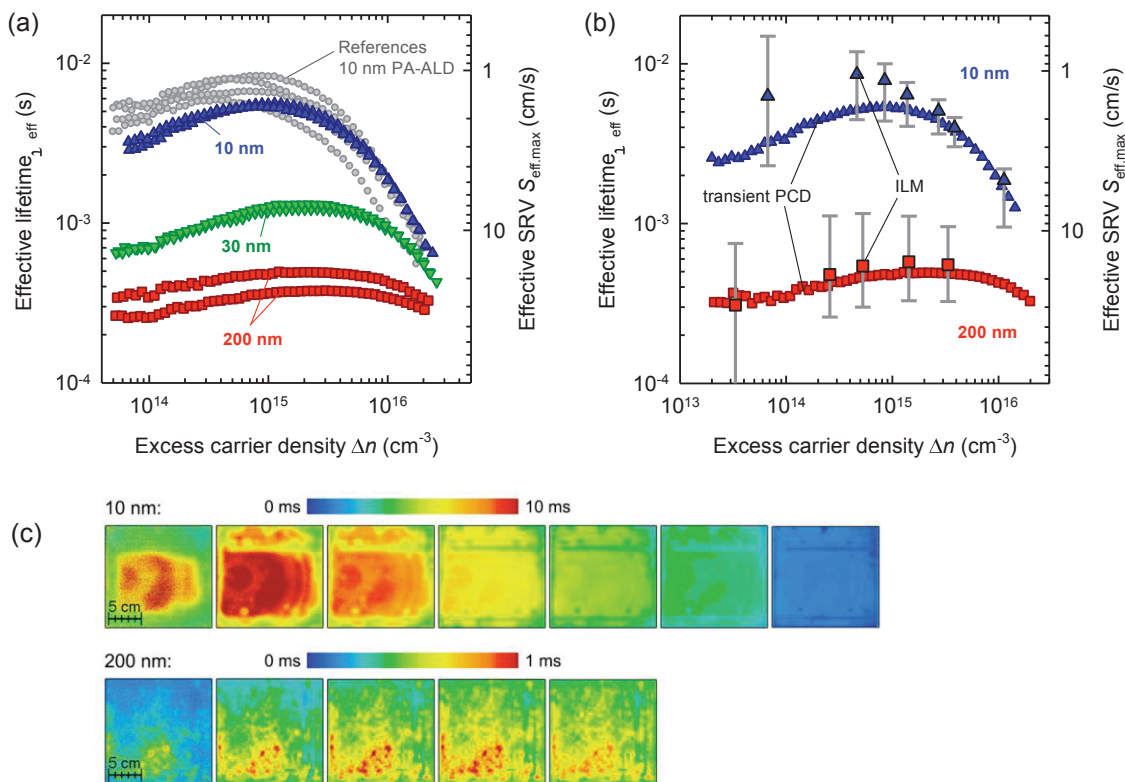


Fig. 3. (a) Effective lifetime τ_{eff} and maximum effective SRV $S_{\text{eff,max}}$ as function of injection density Δn measured by transient PCD. The Al₂O₃ thickness is 10, 30, and 200 nm deposited by spatial ALD, and 10 nm deposited by plasma-assisted ALD, respectively; (b) Comparison of the injection density dependent effective lifetime τ_{eff} and maximum effective SRV $S_{\text{eff,max}}$ as measured by transient PCD and dynamic ILM for two exemplary samples of 10 nm (blue triangles) and 200 nm (red squares); (c) Spatially resolved lifetime mappings measured by dynamic ILM for different illumination intensities for the 10 nm (top row) and 200 nm (bottom row) samples shown in (b). Images are aligned left to right with increasing injection density Δn .

Al₂O₃ thickness all samples only show a minor injection density dependence of the effective lifetime. Taking into account that the same shape of the $\tau_{\text{eff}}(\Delta n)$ curve is observed for all samples including the references passivated by plasma-assisted ALD, the slight decrease in effective lifetime for low injection densities is most likely attributed to the influence of the bulk material. Two samples with an Al₂O₃ thickness of 10 nm (blue triangles) and 200 nm are analyzed in more detail. For these samples Fig. 3(b) shows the $\tau_{\text{eff}}(\Delta n)$ data obtained by transient PCD together with lifetime values extracted from spatially resolved lifetime mappings as described above. Accordingly, each data point in Fig. 3(b) corresponds to a single ILM image in Fig. 3(c). Although a quantitative analysis is beyond the scope of this paper, the minimum lifetime given by the lower error bar appears to drop faster with decreasing injection density Δn than does the maximum lifetime given by the upper error bar. Since the ILM images show a similar spatial lifetime distribution for all injection densities, the injection level dependence of the effective lifetime seems to be independent of spatial position, but is more pronounced in low-lifetime regions.

4. Interface state density of the Si/Al₂O₃ interface

We investigate the interface state density D_{it} at the Si/Al₂O₃ interface as a function of energetic position in the silicon bandgap by capacitance – voltage (C - V) analysis. For the C - V test samples Al₂O₃ was deposited only on the front side of the wafers, which were subsequently laser-cut in 2.5×2.5 cm² pieces. For the C - V measurements the Al₂O₃ layers were not annealed. Circular aluminum gate contacts were defined on top of the Al₂O₃ film by thermal evaporation through a shadow mask. A full-area aluminum back contact was evaporated on the rear side. Figure 4(a) shows the quasi-static and high-frequency capacitances as a function of the applied gate voltage for a 10 nm thick layer of Al₂O₃ deposited by spatial ALD. Both curves are expected to coincide in the accumulation region (for large positive bias), hence the significant difference at 1 V positive bias indicates a measurement problem. As the quasi-static capacitance in accumulation, $C_{\text{QS},0} = 0.50 \mu\text{F}/\text{cm}^2$, agrees very well with the insulator capacitance $C_0 = (0.49 \pm 0.03) \mu\text{F}/\text{cm}^2$ expected from a comparative study (not shown here), the deviation is attributed to a reduced high-frequency capacitance, presumably due to large series and contact resistances. The interface state density D_{it} is extracted from the difference between the quasi-static and the high-frequency capacitance, an erroneously low high-frequency capacitance hence yields an interface state density exceeding the actual value. Taking this into account, the values reported here represent an

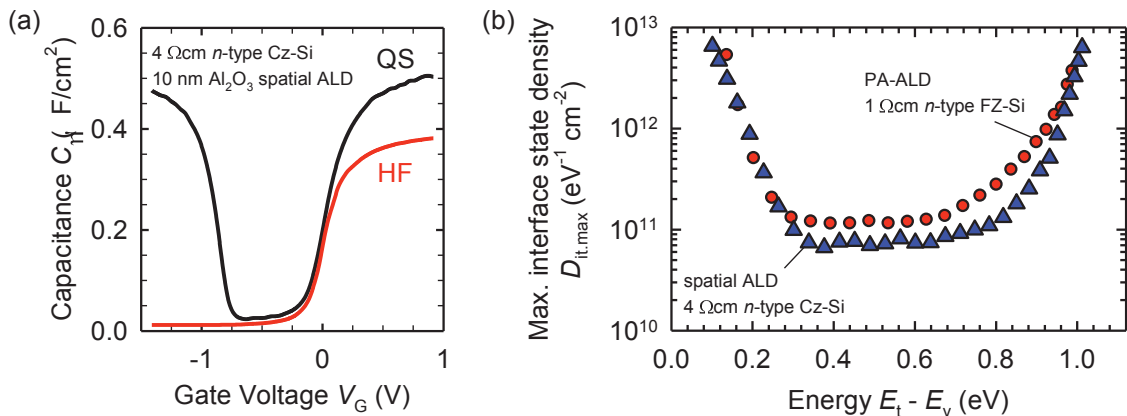


Fig. 4. (a) Quasi-static (QS, black line) and high-frequency (HF, red line) capacitance as a function of applied gate voltage for 10 nm of Al₂O₃ deposited by spatial ALD; (b) Maximum of the interface state density $D_{\text{it,max}}$ as a function of energetic position $E = E_t - E_v$ relative to the silicon valence band edge for 10 nm of Al₂O₃ deposited by spatial ALD (blue triangles). D_{it} values for plasma-assisted ALD on 1 Ωcm n-type float-zone (FZ) Si measured in an earlier experiment [11] (red dots) are given for comparison.

upper bound $D_{it,max}$ to the actual interface state density D_{it} . The maximum interface state density $D_{it,max}$ corresponding to the measurement in Fig. 4(a) is shown in Fig. 4(b) as a function of energetic position $E = E_t - E_v$ of the trap level relative to the silicon valence band edge. Averaged over a range of $\pm 3k_B T$ around the middle of the bandgap we obtain a maximum midgap interface state density of $D_{it,max,midgap} = (7 \pm 1) \times 10^{10} \text{ eV}^{-1} \text{ cm}^{-2}$, which is an exceptionally low value below D_{it} values obtained by plasma-assisted ALD [11].

5. Conclusions

We have demonstrated an excellent level of surface passivation provided by Al_2O_3 deposited by spatial ALD in an inline reactor at a deposition rate of $\sim 30 \text{ nm/min}$. The surface recombination velocity was shown to be virtually independent of injection level, and $S_{eff,max}$ values below 10 cm/s were obtained for Al_2O_3 layers up to 30 nm thickness. An Al_2O_3 passivation layer of 10 nm thickness was shown to yield effective surface recombination velocities $S_{eff,max}$ below 2.9 cm/s and an exceptionally low maximum midgap interface state density of $D_{it,max,midgap} = (7 \pm 1) \times 10^{10} \text{ eV}^{-1} \text{ cm}^{-2}$. We conclude that spatial ALD provides a promising tool for the integration of Al_2O_3 passivation layers into industrial solar cells.

Acknowledgements

Funding was provided by the State of Lower Saxony and the German Ministry for the Environment, Nature Conservation and Nuclear Safety (BMU) under contract number 0325050 (“ALD”).

References

- [1] Agostinelli G, Delabie A, Vitanov P, Alexieva Z, Dekkers H, Wolf SD, Beaucarne G. Very low surface recombination velocities on *p*-type silicon wafers passivated with a dielectric with fixed negative charge. *Solar Energy Materials & Solar Cells* 2006; **90**:3438-3443.
- [2] Hoex B, Heil S, Langereis E, van de Sanden MCM, Kessels WMM. Ultralow surface recombination of c-Si substrates passivated by plasma-assisted atomic layer deposited Al_2O_3 . *Applied Physics Letters* 2006; **89**:042112.
- [3] Dingemans G, Seguin R, Engelhardt P, van de Sanden MCM, Kessels WMM. Silicon surface passivation by ultrathin Al_2O_3 films synthesized by thermal and plasma atomic layer deposition. *Physica Status Solidi – Rapid Research Letters* 2010; **4**:10-12.
- [4] Schmidt J, Merkle A, Brendel R, Hoex B, van de Sanden MCM, Kessels WMM. Surface Passivation of High-efficiency Silicon Solar Cells by Atomic-layer-deposited Al_2O_3 . *Progress in Photovoltaics: Research and Applications* 2008; **16**: 461-466.
- [5] Poodt P, Lankhorst A, Roozeboom F, Spee K, Maas D, Vermeer A. High-Speed Spatial Atomic-Layer Deposition of Aluminum Oxide Layers for Solar Cell Passivation. *Advanced Materials* 2010; **22**: 3564-3567.
- [6] Werner F, Veith B, Tiba V, Poodt P, Roozeboom F, Brendel R, Schmidt J. Very low surface recombination velocities on *p*- and *n*-type c-Si by ultrafast spatial atomic layer deposition of aluminum oxide. *Applied Physics Letters* 2010; **97**: 162103.
- [7] Ramspeck K, Reissenweber S, Schmidt J, Bothe K, Brendel R. Dynamic carrier lifetime imaging of silicon wafers using an infrared-camera-based approach. *Applied Physics Letters* 2008; **93**: 102104.
- [8] Sproul AB. Dimensionless solution of the equation describing the effect of surface recombination on carrier decay in semiconductors. *Journal of Applied Physics* 1994; **76**: 2851.
- [9] Schmidt J, Veith B, Brendel R. Effective surface passivation of crystalline silicon using ultrathin Al_2O_3 films and $\text{Al}_2\text{O}_3/\text{SiN}_x$ stacks. *Physica Status Solidi – Rapid Research Letters* 2009; **3**: 287-289.
- [10] Veith B, Werner F, Zielke D, Brendel R, Schmidt J. Comparison of the thermal stability of single Al_2O_3 layers and $\text{Al}_2\text{O}_3/\text{SiN}_x$ stacks for the surface passivation of silicon. *Energy Procedia* 2011; SiliconPV, Freiburg, Germany.
- [11] Werner F, Veith B, Zielke D, Kühnemund L, Tegenkamp C, Seibt M, Brendel R, Schmidt J. Electronic and Chemical Properties of the c-Si/ Al_2O_3 Interface. *Journal of Applied Physics* 2011; in press.